JTTEE5 16:84–95
DOI: 10.1007/s11666-006-9009-0
1059-9630/$19.00 © ASM International

Peer Reviewed

Nonlinear Behavior in Compression and Tension of Thermally Sprayed Ceramic Coatings

F. Kroupa

(Submitted May 23, 2006; in revised form September 12, 2006)

Mechanical properties of thermally sprayed coatings, especially of ceramics, are strongly influenced by a high density of mesoscopic defects, microcracks of dimensions between fractions of μm up to tens of μm. The anisotropic linear elastic stress–strain relations are valid only at very low deformations, e.g., $|e| < 0.05\%$, with small values of Young's moduli due to elastic openings and elastic partial closings of microcracks. At higher deformations, e.g., $0.05\% < |e| < 0.4\%$, the stress–strain relations are strongly nonlinear. Under compressive stresses, elastic closing of microcracks leads to a gradual decrease of the microcrack density and to an increase of Young's modulus in compression. Under tensile stresses, the microcracks slightly grow by inelastic processes; the microcrack density gradually increases and effective Young's modulus in tension decreases. A two-parametric equation containing linear and quadratic terms is used to describe the nonlinear stress–strain curves of plasma-sprayed ceramic coatings. The effect of nonlinearity on the bending of beams with coatings and the nonlinear combination of external and residual stresses are discussed. The fracture of coatings at higher tensile stresses due to coalescence of the microcracks is mentioned.

Keywords compression and tension, fracture, microcracks, nonlinear behavior, plasma-sprayed ceramics, residual stresses, Young's moduli

1. Introduction

Thermal spraying is a process in which the material usually in a powder form is melted, accelerated to a high velocity and deposited on the substrate. Different techniques of thermal spraying are used; e.g., plasma spraying, detonation-gun spraying, high velocity oxy-fuel spraying, etc. (Ref 1).

The microstructure of sprayed materials is complex. It consists of irregular thin lamellae known as ''splats'', formed by rapid solidification of the impacted molten droplets, of diameters between 100 and 300 μm and heights between 2 and 10 μm. For the spraying direction $-x_3$, the splats are approximately parallel to the spraying plane, x_1x_2. The splats are polycrystalline and consist usually of irregular fine columnar grains, elongated approximately in the x_3 direction. Imperfect bonds between the splats and substrate and between the individual splats develop during the rapid cooling.

The total porosity of the sprayed materials is usually between 2 and 15%, and is mostly due to four families of defects (Fig. 1):

- irregular pores between the splats
- spherical pores inside the splats
- imperfect bonding between the splats along the interfaces approximately parallel to the spraying plane x_1x_2; the unbonded regions are referred to as thin intersplat voids (intersplat or horizontal microcracks or briefly cracks)
- microcracks approximately perpendicular to the spraying plane x_1x_2 formed inside the splats during their rapid cooling after solidification. They form an irregular microcrack pattern with microcrack normals distributed in the x_1x_2 planes, and are referred to as intrasplat microcracks (vertical microcracks or briefly cracks)

Although the intersplat and intrasplat microcracks represent only a small part of the total porosity, they are believed to be the main factor causing the decrease of Young's moduli (due to elastic openings and partial closings of the microcracks under small stresses) and the elastic anisotropy. The intersplat cracks lead to the decrease of Young's modulus E_3 in the spraying direction x_3, while the intrasplat cracks lead to the decrease of Young's moduli E_1 in the directions lying in the x_1x_2 plane. This effect is more pronounced in ceramic than in metallic materials (Ref 1).

High macroscopic residual stresses usually appear in thermally sprayed coatings (Ref 2). They can be divided into three groups from the point of view of their origin:

- Quenching (or primary) residual stresses develop during the deposition process through a fast thermal contraction of solidified splats: they cool from the

F. Kroupa, Institute of Plasma Physics of ASCR, Za Slovankou 3, 182 21, Prague 8, Czech Republic. Contact e-mail: kroupaf@ipp.cas.cz

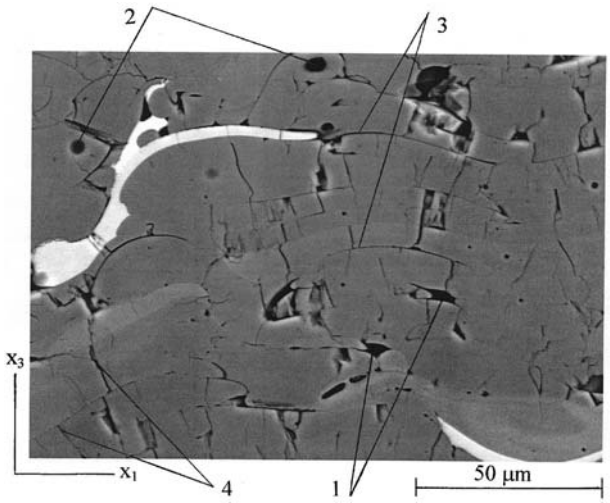

Fig. 1 Microstructure of plasma-sprayed gray alumina ($Al_2O_3 + 3\%$ TiO_2, vertical cross-section) White areas: TiO_2, (1) Irregular pores between the splats, (2) Spherical pores inside the splats, (3) Intersplat thin voids (intersplat or horizontal microcracks), (4) Intrasplat (vertical) microcracks. (SEM, B. Kolman, Institute of Plasma Physics, Prague)

melting point down to the relatively low deposition temperature; i.e., the temperature of the substrate and of the previously deposited splats. The quenching stresses are tensile and only slightly depend on the substrate properties.

- Differential thermal contraction (or secondary) residual stresses appear when the substrate with the completed coating is cooled from the deposition temperature (usually a few hundred °C) to the ambient temperature. The secondary stresses depend on the difference of thermal expansion coefficients of the coating and substrate and can be tensile or compressive.
- In metal coatings deposited with a high velocity of the impacted droplets (e.g., by detonation spraying) also peening compressive stresses are produced.

The resulting residual stresses are sensitive to the parameters of the spraying technology used, and may be a function of the distance x_3 from the interface, especially in thick coatings. There is a close connection between the quenching stresses and intrasplat cracks. The thermal contraction of the splats due to cooling from the melting temperature to the deposition temperature is of the order of 1%, and the corresponding quenching stresses would be high, of the order of a few GPa. However, the majority of these stresses relax during cooling, in metals mostly by plastic deformation and in ceramics preferentially by microcracking. Therefore, intrasplat cracks are formed as a process of relaxation of the quenching stresses. The residual quenching stresses are usually smaller in ceramics than in metals.

A typical thickness of thermally sprayed coatings is between 0.2 mm and 1 mm. However, also free-standing parts are manufactured by thermal spraying, usually by air plasma spraying of ceramics. They are prepared as thick coatings (of thickness up to 10 mm) and the substrate is then removed, e.g., by dissolution or by separation along the interface (Ref 3). The distribution of microcracks in the free-standing parts remains the same as in the coatings; however, the residual stresses partly relax and partly redistribute during separation.

Microcracks of high density influence considerably various properties of sprayed materials, some of them in a negative way, but some in a positive way. The delamination of coatings under external loading, by thermal stresses and also by residual stresses, proceeds by interconnection of microcracks in the interface. Fracture proceeds by interconnection of intrasplat cracks. On the other hand, elastic openings of the intrasplat cracks (leading to smaller Young's moduli) allow the ceramic coating to follow the tensile deformation of the substrate to deformations $\approx 0.2\%$ without formation of macroscopic cracks. The microcracks improve the thermal-shock resistance of sprayed materials. The intersplat cracks decrease the thermal conductivity of sprayed coatings and improve their function as thermal barriers (Ref 1).

In the previous literature on mechanical properties of thermally sprayed materials, the main attention was paid to small values of Young's moduli, to the elastic anisotropy at low stresses and to fracture at high tensile stresses (Ref 1). In this paper, the nonlinearity of the mechanical behavior of thermally sprayed ceramics at medium stresses will be emphasized. Comments on the present theoretical models of the approximately linear elastic behavior at low stresses will first be given. A nonlinear elastic behavior under higher compressive stresses and nonlinear inelastic behavior under higher tensile stresses will be analyzed. A two-parametric equation containing linear and quadratic terms of strain will be proposed to describe the nonlinear stress–strain curves of plasma-sprayed ceramic coatings. The effect of the nonlinearity on bending of substrates with coatings, and the nonlinear combination of external and residual stresses will be discussed. The transition to fracture at high tensile stresses, due to coalescence of microcracks, will be mentioned.

2. Summary of the Linear Elastic Behavior at Low Stresses

The experiments show that coatings and freestanding parts manufactured by thermal spraying have much smaller elastic stiffness constants (measured at low stresses), twice up to three times less for metals and three to ten times less for ceramics, than the corresponding well sintered materials. Moreover, they have different Young's moduli E_1 and E_3 in the directions parallel and perpendicular to the spraying plane (Ref 1).

A number of theoretical papers (Ref 4-7) explaining the low values of elastic moduli have already been published. The material of the splats is considered as a linear elastic isotropic continuum characterized by two elastic constants, Young's modulus E_0 and Poisson's ratio ν_0. The

microcracks are modeled as flat hollow rotational ellipsoids (called circular cracks), randomly distributed in the continuum as two families: intersplat cracks parallel to the x_1x_2 plane and intrasplat cracks with normals randomly distributed in the x_1x_2 planes (Fig. 2). Also a small effect of approximately spherical pores is taken into account. The material is anisotropic with the transverse isotropy (Ref 8), characterized by five independent elastic constants. The cracks are assumed to be sufficiently opened so that the same elastic behavior in tension and compression follows.

The linear Hooke's law between small deformations e_{ij} and small stresses σ_{ij} can be written generally (using the reduced index notation (Ref 8)) in the form

$$e_i = \sum_{j=1}^{6} S_{ij}\,\sigma_j, \quad i = 1,2,\ldots,6 \qquad \text{(Eq 1)}$$

where S_{ij} are the elastic compliance constants (it is, e.g., $e_1 = e_{11}$, $\sigma_1 = \sigma_{11}$, $S_{11} = 1/E_1$, $e_6 = 2e_{12}$, $\sigma_6 = \sigma_{12}$, $S_{66} = 1/G_{12}$).

For the transverse isotropy with respect to the x_1x_2 plane, it is:

$$\begin{aligned} S_{11} &= S_{22} = 1/E_1,\ S_{33} = 1/E_3 \\ S_{12} &= S_{21} = -\nu_{12}/E_1,\ S_{31} = S_{32} = S_{13} = S_{23} \\ &= -\nu_{31}/E_3 = -\nu_{13}/E_1 \\ S_{44} &= S_{55} = 1/G_{13},\ S_{66} = [2(1+\nu_{12})]/E_1 \end{aligned} \qquad \text{(Eq 2)}$$

with five independent elastic constants: E_1 (Young's modulus in the isotropic x_1x_2 plane), E_3 (Young's modulus in the x_3 direction), ν_{12}, ν_{31}, and G_{13}. The defect structure of the sprayed materials can be modeled by spherical pores of radii R_k and by circular cracks of radii r_{1k} and r_{3k} (Fig. 2). The porosity P, $0 < P << 1$, is mainly due to irregular, approximately spherical pores between the splats, and to smaller extent to spherical pores inside the splats. The effect of cracks on the elastic constants can be characterized by the so-called scalar crack densities ρ per unit volume (Ref 5-7,9,10), in our case by ρ_1 and ρ_3. They can be expressed as

$$\begin{aligned} P &= (1/V)\sum_{k=1}^{n} (4/3)\,\pi R_k^3 \\ \rho_1 &= (1/V)\sum_{k=1}^{m} r_{1k}^3,\ \rho_3 = (1/V)\sum_{k=1}^{q} r_{3k}^3 \end{aligned} \qquad \text{(Eq 3)}$$

The effect of cracks is not given by their areas (proportional to r^2), but by the "adjoined volumes" proportional to r^3 (Ref 9): a larger crack has a larger effect than smaller cracks of the same total area. The dependence of the five elastic constants on P, ρ_1 and ρ_3 can be constructed using the results of papers (Ref 5,9,10) as a sum of the effects of porosity and scalar crack densities. Only the results for the Young's moduli E_1 and E_3 from (Ref 5) will be given here:

$$\begin{aligned} E_1 &= E_0/\{1 + c_1\,P/(1-P) + a_1\,\rho_1/(1-P)\} \\ E_3 &= E_0/\{1 + c_3\,P/(1-P) + a_3\,\rho_3/(1-P)\} \end{aligned} \qquad \text{(Eq 4)}$$

where the positive constants c_1, a_1, c_3 and a_3 depend on Poisson's ratio ν_0:

$$\begin{aligned} c_1 &= c_3 = 3(1-\nu_0)(9+5\nu_0)/[2(7-5\nu_0)] \\ a_1 &= 8(1-\nu_0^2)(1-3\nu_0/8)/[3(1-\nu_0/2)],\ a_3 = 16(1-\nu_0^2)/3 \end{aligned} \qquad \text{(Eq 5)}$$

The interaction between pores and cracks is taken into account in Eq 4 in a simplified way in the scheme of the effective stress field, and is expressed by terms $1/(1-P)$ (Ref 9,10).

For fixed porosity P and crack densities ρ_1 and ρ_3, the Young's moduli in Eq 4 can be taken as a first approximation for small deformations e_{ij} and small stresses σ_{ij}.

As an example, the dependence of E_1/E_0 on the scalar crack density ρ_1 is shown in Fig. 3 for three values of porosity P and three values of Poisson's ratio ν_0.

The modeling of microcracks as a distribution of flat hollow rotational ellipsoids (Ref 4-7) is far from the real microcrack distribution, shown in Fig. 1. Rather, the intersplat boundary structure reminds of islands of good bonding, surrounded by interconnected unbonded regions (intersplat microcracks) of complicated shapes (Ref 11). The intrasplat microcracks form irregular nets of microcracking inside the splats. Nevertheless, the models developed in Ref 4-7 can be considered as useful simplified theoretical models which can be treated analytically and which explain in principle the small values of Young's moduli and elastic anisotropy of thermally sprayed materials.

There is a high number of measurements of Young's modulus E_1 and a smaller number of measurements of E_3, and the total porosity P is also usually determined (Ref 1). On the other hand, there are only a few attempts to estimate the densities and dimensions of microcracks. The unbonded areas between the splats and intrasplat microcracks were made visible in sprayed alumina by copper decoration (Ref 12) and the fraction of the unbonded areas was estimated as large as 70%. The total surface areas of all cracks and pores of the order of 10^6 m^2/m^3 (i.e., 1 $\mu m^2/\mu m^3$) were measured in plasma-sprayed zirconia and alumina by small-angle neutron scattering in a series of papers by Ilavsky et al., e.g., in Ref 13. A quantitative comparison of the theoretical predictions with experimental results is proposed in Ref 14,15.

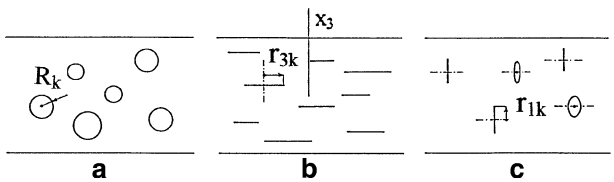

Fig. 2 Theoretical model of the defect structure: (a) spherical pores, (b) horizontal microcracks (c) vertical microcracks (Ref 5)

3. Nonlinear Behavior in Uniaxial Compression and Tension

The sprayed materials could be considered as the so-called bimodular materials, i.e., the materials with

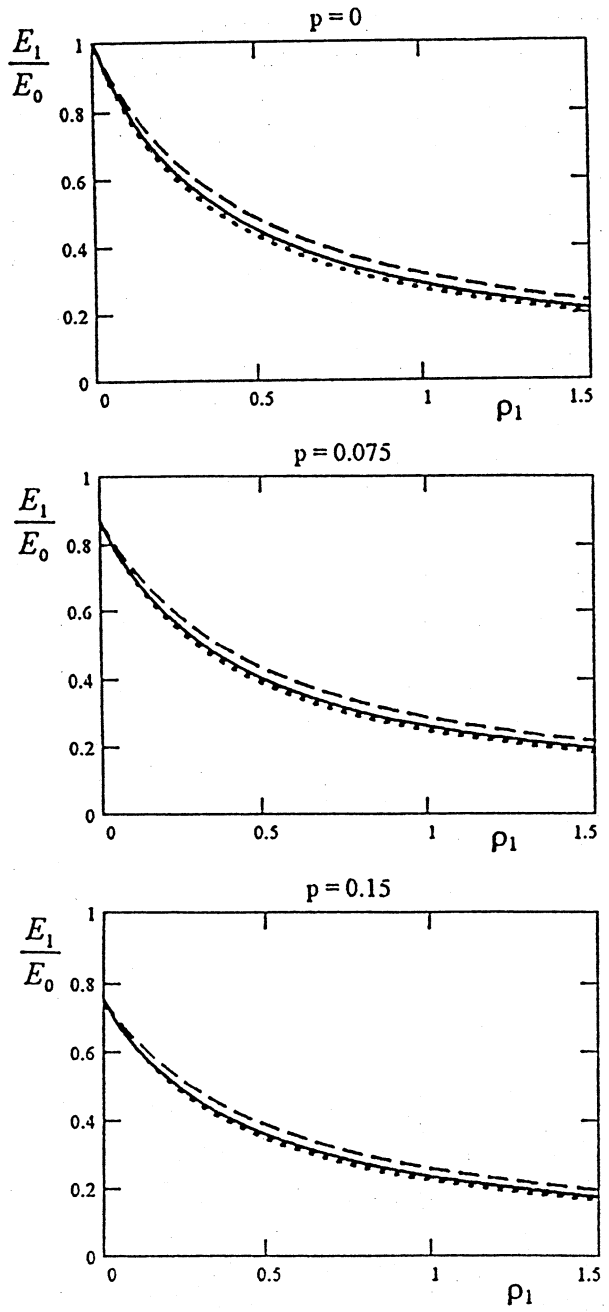

Fig. 3 Dependence of $E_1(\rho_1)/E_0$ for porosities $p = 0$, $p = 0.075$, and $p = 0.15$. Full curves: $\nu_0 = 1/3$; dotted curves: $\nu_0 = 0$; dashed curves: $\nu_0 = 1/2$ (Ref 5)

different Young's moduli under tension and compression (Ref 16). Moreover, their behavior in tension and in compression is strongly nonlinear.

A similar strong nonlinear behavior in compression is known in geophysics. The effect of hydrostatic pressure on the velocity of elastic waves, which depends on elastic constants, is an important phenomenon in geophysics. In the theoretical papers (Ref 17,18) this effect is explained by the closing of cracks present in the rocks, although usually to a smaller extent than in plasma-sprayed ceramics. Under hydrostatic pressure the bulk modulus of rocks increases, and the effect is found to be purely elastic and reversible (Ref 17). On the other hand, under uniaxial compression Young's modulus of rocks also increases with compressive stress; however, the effect is not purely elastic and inelastic hysteresis appears during stress cycling (Ref 18). This is explained by the relative shear displacements along the surfaces of cracks forming different angles with the stress axis, which leads to friction and energy absorption. These effects have been experimentally confirmed (Ref 17-20) and are well recognized in geophysics.

Similar but more pronounced effects of compressive external or residual stresses on elastic moduli appear in thermally sprayed materials, especially in plasma-sprayed ceramics with high density of microcracks, as discussed first in Ref 21 and analyzed theoretically in (Ref 22-24). In these papers, the nonlinear behavior in compression (increase of Young's moduli wih compressive stresses) is explained for anisotropic materials by the decrease of crack densities ρ_1 and ρ_3, by elastic closing of microcracks due to compressive stresses; i.e., by the dependences $\rho_1(\sigma_1)$ and $\rho_3(\sigma_3)$. However, these dependences are not yet known from experiments nor from theory and were chosen in Ref 22-24 to get agreement with experiments, e.g., in Ref 25,26.

In contrast to geophysics, the nonlinearity at tensile stresses is also important in coatings. However, the growth of microcracks due to tensile stresses, leading to decrease of Young's moduli, is an inelastic process, which is more complex than the elastic closing of microcracks by compressive stresses. No attempt to study this process generally in anisotropic materials has been published, and no dependences $\rho_1(\sigma_1)$ and $\rho_3(\sigma_3)$ discussed for tensile stresses.

To describe the nonlinear behavior of coatings, a significant simplification of the nonlinear theory of elasticity is used: only the physical nonlinearity is considered, i.e., the stress-strain relations are nonlinear. On the other hand, the geometrical linearity is applied, i.e., the strain components e_{ij} are assumed small, $|e_{ij}| << 1$, and the relations for strains $e_{ij} = (1/2)(\partial u_i/\partial x_j + \partial u_j/\partial x_i)$ (where u_i are the displacement components) following from the linear theory of elasticity are used (Ref 27). In spite of the considerable physical nonlinearity, the strain components in coatings remain very small, $|e_{ij}| < 10^{-2}$.

Sprayed ceramic coatings on (usually metal) substrates are deformed under strain-driven loading (controlled by the substrate deformation) and retain their integrity by constraint due to the substrate up to tensile deformations between 0.2 and 0.4%, when macroscopic cracks start to form by interconnection of microcracks. There is a continuous transition from nonlinear deformation to macrocrack formation.

The nonlinear behavior under tension may have various origins:

- Some microcracks with their faces in contact, however, without bonding, may gradually elastically open with increasing tensile stress. This will lead to a gradual

increase of the effective microcrack density by a purely elastic process and to elastic nonlinearity: with increasing tensile stress, Young's moduli will decrease.

- Under uniaxial stress, there are also shear stresses along some microcracks which may lead to relative displacements with local friction, energy absorption and inelastic contribution.
- Moreover, some local bonds may be so weak that they can be broken even at small tensile stresses. Therefore, some microcracks can grow or new microcracks can be formed and this process leads to a small increase of the microcrack densities and to a small energy absorption.

The effective Young's modulus will decrease during the tensile loading; however, some microcracks will again close during unloading and a hysteresis curve should be measured during a cyclic tensile loading. The corresponding contribution to nonlinearity can be called inelastic.

At larger tensile stresses, macroscopic cracks are formed by interconnection of microcracks and permanent irreversible damage starts to form inside the material as a process preceding fracture.

Some systematic measurements of the nonlinear processes under a higher tensile deformation, preceding fracture in plasma-sprayed ceramics, were started recently (Ref 28).

A simple nonlinear stress–strain relation which could agree with these experiments will be proposed. An empirical relation used in (Ref 23) for uniaxial elastic compression will be employed and extended to inelastic tensile deformation. It will be taken in the form

$$\sigma = E_1 (e - \mathrm{K}\, e^2) \text{ for } -0.5 \times 10^{-2} < e < 1/\mathrm{K},$$
$$\sigma = 0 \text{ for } e > 1/\mathrm{K} \qquad \text{(Eq 6)}$$

The values of the new dimensionless material constant K characterizing the nonlinearity can be expected in the region $50 < K < 200$ for sprayed metals and $200 < \mathrm{K} < 600$ for sprayed ceramics (Ref 23). It may be different for deformation in the x_1x_2 plane for $\sigma_1(e_1)$ and in the x_3 direction for $\sigma_3(e_3)$. In some cases, the value of K might be different for elastic compression and inelastic tension. The limit value for compressive deformations, -0.5×10^{-2}, is chosen rather arbitrarily as it depends on the material. For larger compressive deformations, most cracks become closed and linear elastic behavior with Young's modulus close to E_0 follows. The values of K can be fitted so as to give a good agreement with experimental $\sigma(e)$ curve in compression as well as in tension from papers (Ref 25,28).

The stress–strain relation (6) is plotted in Fig. 4 for different values of K. The maximum possible value of tensile stresses follows from condition $d\sigma/de = 0$, i.e., $\sigma_{MAX} = E_1/(4K)$ for $e_{MAX} = 1/(2K)$.

Tangent modulus $E^{TAN} = d\sigma/de$ and secant modulus $E^{SEC} = \sigma/e$ follow from Eq 6 as

$$E^{TAN}/E_1 = 1 - 2\,Ke$$
$$E^{SEC}/E_1 = 1 - Ke, \; -0.5 \times 10^{-2} < e < 1/\mathrm{K} \qquad \text{(Eq 7)}$$

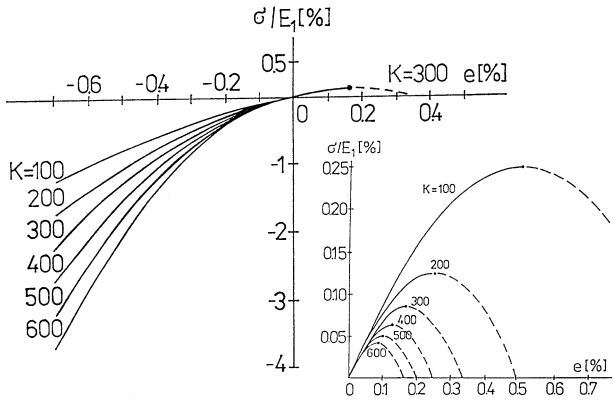

Fig. 4 Nonlinear stress–strain relation (Eq. 6) for different values of material constant K. The tension region is depicted in detail

They have a similar meaning as Young's moduli for elastic compression; however, they only describe the shape of the inelastic stress-strain curve in tension and will be called simply tangent and secant (effective) moduli. They can also be expressed as functions of stress σ because deformation e can be calculated from the algebraic quadratic Eq 6 as a function of σ.

The moduli are plotted in Fig. 5(a), and (b) as functions of normalized deformation $2Ke$ and of dimensionless stress $4\mathrm{K}\sigma/E_1$. They are also denoted as functions of e and σ for K = 300 and $E_1 = 50$ GPa.

The proposed nonlinear relation $\sigma(e)$, Eq 6, and the dependence $E^{TAN}(\sigma)$ can be compared with recent experiments.

The $\sigma(e)$ relation was measured for plasma-sprayed ceramic coatings on the compression or tension side of a steel substrate deformed by bending (Ref 28). Stress σ and strain e were evaluated in the central plane of the coating and the experimental curve for Al_2O_3 coating is reproduced in Fig. 6(a). The full curve corresponds to loading and the dashed curve to unloading. There is a moderate hysteresis under compression and a strong hysteresis under tension. The experimental curve is compared with the proposed $\sigma(e)$ relation, (Eq 6), with $E_1 = 20$ GPa and constant K = 300.

Ultrasound velocities under increasing uniaxial compression in plasma-sprayed freestanding ceramic specimens were measured in Ref 25. Elastic stiffness constants $C^{TAN}{}_{11}$ were then evaluated and tangent moduli estimated from the relation $E^{TAN} \cong 0.8\ C^{TAN}{}_{11}$. The experimental dependence $E^{TAN}(\sigma)$ for Al_2O_3 is plotted in Fig. 6(b) and compared with the theoretical curves from Fig. 5(b) for $E_1 = 40$ GPa and three values of constant K.

The dependence of Young's modulus on compressive and tensile stresses was also shown, e.g., in Ref 29 from bending tests for thermal barrier coatings (ZrO_2 + 7-8 wt.% Y_2O_3) on superalloy substrates. Free-standing coatings were deformed in pure tension and pure compression in Ref 30, and dependences of Young's moduli on stress were found.

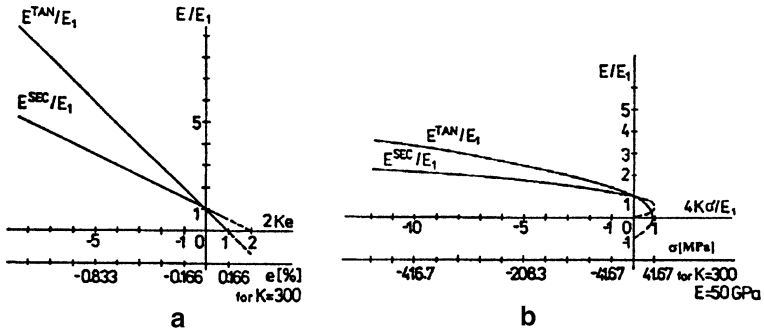

Fig. 5 Dependence of the dimensionless tangent and secant moduli on: (a) Normalized deformation (Eq. 7), (b) Dimensionless stress. The moduli are also given in dependence on deformation e and stress σ for K = 300 and $E_1 = 50$ GPa

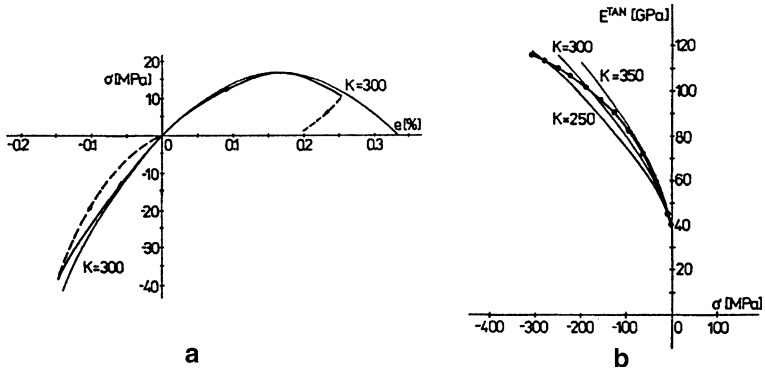

Fig. 6 (a) Comparison of experimental curve $\sigma(e)$ for Al_2O_3 coating after (Ref 28) with theoretical relation (Eq. 6) for K = 300. (b) Comparison of $E^{TAN}(\sigma)$ dependence in compression for Al_2O_3 , based on experiments in Ref 25, with the theoretical relation (Eq. 7) for three values of constant K

The agreement between the experimental and theoretical curves is not perfect; however, there is a good qualitative agreement for tension as well as for compression.

Similar nonlinear effects should appear for other physical properties of coatings influenced by the presence of microcracks. For example, thermal conductivity λ of sprayed thermal barrier coatings, usually ZrO_2 + 8%Y_2O_3, is only $\lambda \cong 0.5$ Wm^{-1} K^{-1} in the direction normal to the interface; i.e., about four times smaller than the value for the well-sintered material, $\lambda \cong 2$ Wm^{-1} K^{-1} (Ref 1). This effect is due to the imperfect bonding between the splats, i.e., to the intersplat microcracks. Therefore, thermal conductivity λ should increase under uniaxial pressure acting on the coating plane (or under hydrostatic pressure), leading to the gradual elastic closing of intersplat microcracks and to the effective decrease of their density.

Two cases of application of Eq. 6 will be discussed, nonlinear bending and nonlinear combination of external and residual stresses.

4. Bending of Beams with Nonlinear Coatings

Pure bending due to initial deformation ε in the coating and due to external moment M (per unit thickness in the $x_2 = y$ direction, Fig. 7) will be studied as a plane stress problem. The initial deformation may be attributed, e.g., to the secondary (differential thermal contraction) residual stresses caused by cooling of the coating with substrate from temperature T to reference temperature T_0, $T > T_0$. Homogeneous initial deformations in the x_1 direction in the coating and the substrate are $\varepsilon = \alpha\,(T_0 - T)$, $\varepsilon_S = \alpha_S\,(T_0 - T)$, where α and α_S are the constant thermal expansion coefficients of the coating and substrate, respectively. For simplicity, we assume in the further text that in the coating $\varepsilon = (\alpha_S - \alpha)(T - T_0) = \text{constant}$, while in the substrate $\varepsilon_S = 0$, without loss of generality.

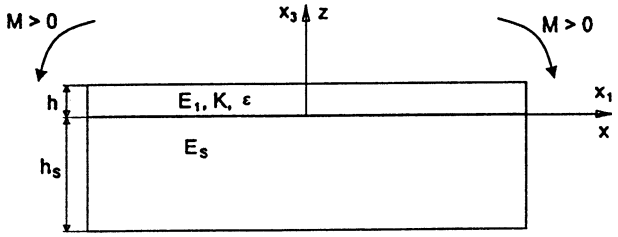

Fig. 7 Bending of a beam by initial deformation ε in the coating and by external moment M

In view of compatibility equations, the total strain in the $x_1 = x$ direction, $e^{T}_{xx} = e_T$, must be a linear function of coordinate $x_3 = z$ and will be written as

$$e_T = A(z/h) + B, -h_S \le z \le h \quad \text{(Eq 8)}$$

where h and h_S are the thicknesses of the coating and substrate, respectively. A and B are dimensionless constants, which can be determined from the equilibrium conditions.

Elastic deformations ε in the x direction in the coating and substrate are given by

$$e = e_T - \varepsilon = A(z/h) + B - \varepsilon,\ 0 < z \le h$$
$$e = e_T = A(z/h) + B, -h_S \le z < 0 \quad \text{(Eq 9)}$$

A homogeneous isotropic elastically linear substrate with Young's modulus E_S is considered, by assuming

$$\sigma = E_S e,\ -h_S \le z < 0 \quad \text{(Eq 10)}$$

A nonlinear elastic stress–strain relation for the coating will be taken in the form given by Eq 6. The unknown constants A and B can be calculated from the conditions of equilibrium of forces and moments over any cross-section $x =$ constant:

$$\int_{-h_s}^{0} \sigma(z)dz + \int_{0}^{h} \sigma(z)dz = 0 \quad \text{(Eq 11)}$$

$$\int_{-h_s}^{0} \sigma(z)zdz + \int_{0}^{h} \sigma(z)zdz = M \quad \text{(Eq 12)}$$

where in the first and second integrals $\sigma(z)$ is given by Eq 6 and 10 (with 9), respectively.

The integrals in (Eq 11) and (Eq 12) are elementary and can be evaluated analytically. Equations 11 and 12 then transform into a system of two nonlinear algebraic equations for two unknown constants; A and B,

$$3D[-H^2A + 2HB] + 3A + 6(B - \varepsilon) - 2K[A^2 + 3A(B - \varepsilon) + 3(B - \varepsilon)^2] = 0 \quad \text{(Eq 13)}$$

$$2D[2H^3A - 3H^2B] + 4A + 6(B - \varepsilon) - K[3A^2 + 8A(B - \varepsilon) + 6(B - \varepsilon)^2] = 12m \quad \text{(Eq 14)}$$

where dimensionless quantities have been introduced:

$$D = (E_S/E_1),\ H = (h_S/h),\ m = M/(E_1h^2) \quad \text{(Eq 15)}$$

Solving for A and B, the stresses $\sigma(z)$ follow from Eq. 6 and 10 with Eq. 9. The radius of curvature R of the beam can be calculated as $R = h/A$.

The solution for a linear coating, i.e., for $K = 0$, was established by several authors, e.g., in Ref 31. For this simple case, Eq. 13 and 14 transform into a system of two linear algebraic equations for A and B which can be solved analytically.

In case $K \neq 0$, Eq. 13 and 14 for constants A and B cannot be solved analytically. Therefore, the solution for a nonlinear coating was performed numerically (Ref 31) by mathematical software package MAPLE (Maple 6, Waterloo Maple Inc., Ontario, Canada) and the MAPLE built-in function *fsolve* was used.

Numerical solution (Ref 31) was carried out for the ratio of Young's moduli $D = (E_S/E_1) = 4$ as a typical value for a ceramic coating (e.g., Al_2O_3) on a steel substrate. Two values of the thickness ratio $H = (h_S/h)$, $H = 2$, and $H = 5$, were chosen as typical values of thick and thin coatings. The values of the material constant K (taken as equal under compression and tension) were chosen as $K = 0$ (linear coating), 200, 300, 400. The results are expressed in the form of tables for constants A and B and of graphs $\sigma(z/h)$ where the dimensionless coordinate $(z/h) = t$ is introduced. It is possible to represent the stresses in dimensionless form as (σ/E_1) without specifying the value of Young's modulus E_1; however, the values of stresses $\sigma(t)$ in MPa are directly given in the graphs for $E_1 = 50$ GPa (ceramic coating) and $E_S = 200$ GPa (steel substrate).

Only three examples will be given here for $D = 4$, $H = 5$, and $K = 300$: stresses due to initial deformations ε only (i.e., for $m = 0$) in Fig. 8, stresses due to external moments m only (i.e., for $\varepsilon = 0$) in Fig. 9 and stresses due to a combination of ε and m in Fig. 10. The values of $\varepsilon > 0$ and $m < 0$ lead to compressive stresses. Similar results for compressive stresses for another $\varepsilon(\sigma)$ relation were obtained (Ref 32). The results for linear solution ($K = 0$) are shown by dashed curves so that the effect of nonlinearity is visible. Note that in the nonlinear treatment the combined case in Fig. 10 is not equal to the sum of the special cases.

The importance of the nonlinear combination of the residual and external stresses will be illustrated on the simple case of a thin coating on a thick substrate where an analytical solution can be obtained even for the nonlinear case.

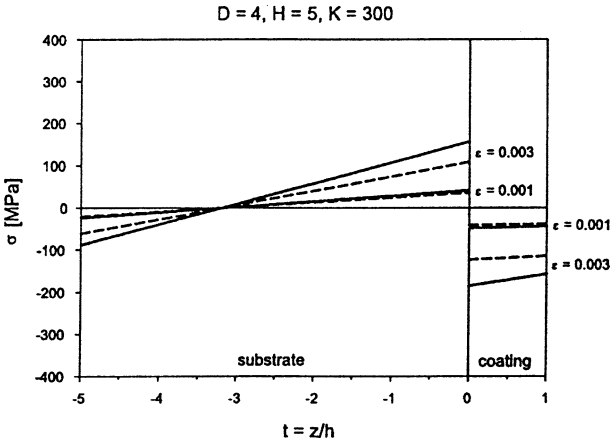

Fig. 8 Compressive residual stresses in coatings on substrates due to initial deformations $\varepsilon = 0.001$ and $\varepsilon = 0.003$. Full lines correspond to the nonlinear solution, dashed lines to the linear solution ($D = 4$, $K = 300$, $H = 5$) (Ref 31)

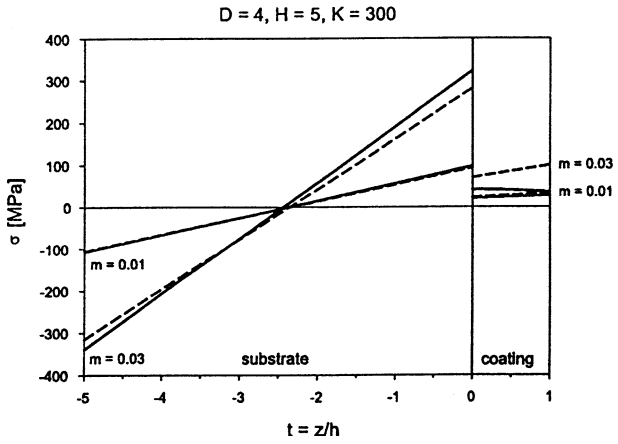

Fig. 9 Tensile external stresses due to dimensionless moments m ($D = 4$, $K = 300$, $H = 5$, $m = 0.01$ and $m = 0.03$) (Ref 31)

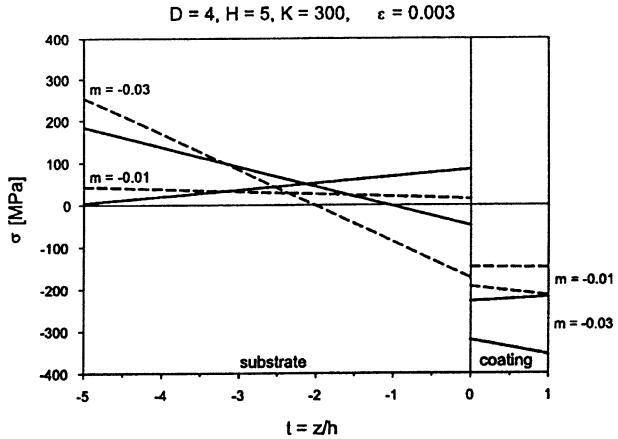

Fig. 10 Combination of compressive residual stresses with compressive external stresses ($D = 4$, $K = 300$, $H = 5$, $\varepsilon = 0.003$, $m = -0.01$, and $m = -0.03$) (Ref 31)

5. Nonlinear Combination of Residual and External Stresses

The macroscopic residual stresses act in the directions parallel to the spraying plane x_1x_2 (Fig. 7), $\sigma_{11R} \approx \sigma_{22R}$ while $\sigma_{33R} \approx 0$. In thin coatings, the residual stresses are approximately constant.

Some comments will be given on the effect of residual stresses on the Young's moduli and on the nonlinear behavior of sprayed coatings with residual stresses. Plane stress problem will be assumed for simplicity.

Residual stresses σ_{11R}, have the same effect on the intrasplat (vertical) microcracks inside the splats as external stresses σ_{11}. Therefore, under compressive residual stresses σ_{11R}, some intrasplat cracks will be closed and Young's modulus E_1, measured under small external stresses, will be higher than that of the material without residual stresses. Under tensile residual stresses σ_{11R}, the density of intrasplat microcracks increases and Young's modulus E_1 will be smaller than in the case without residual stresses.

Two types of bending experiments are used for characterization of coatings:

- From the measured radius of curvature of specimens without external moments, the residual stresses in the coatings can be determined.
- From the measured radius of curvature under external moment, the Young's modulus E_1 of the coating can be determined.

For the linear case the superposition of residual and external stresses is linear. On the other hand, in the nonlinear case the combination of nonlinear residual and external stresses is also nonlinear, and this has an important consequence. If the stress–strain relations or elastic constants are measured under external loading in specimens with (known or unknown) residual stresses, the results will depend on these residual stresses and will differ from those in the specimen without residual stresses.

This result will be illustrated on the simple case of a thin coating on a thick substrate where an analytical solution can be obtained even for the nonlinear case, based on Eq 6.

In a thin coating on a thick substrate, the stress in the coating only slightly depends on coordinate $x_3 = z$ and can be taken as approximately constant for $h << h_S$, where h and h_S are the thicknesses of the coating and substrate, respectively:

- For a given homogeneous initial deformation ε_R (without external stresses), the corresponding elastic deformation e_R is also homogeneous, $e_R = -\varepsilon_R$, because the substrate practically does not deform and total deformation in the coating $e_T = \varepsilon_R + e_R = 0$. The constant residual stress σ_R follows from Eq 6 as $\sigma_R = E_1(e_R - Ke_R^2)$.
- For a given homogeneous external deformation e_{EXT} (without residual stresses) induced by the elastic deformation of the substrate, $e_{EXT} < 1/(2K)$, external stress σ_{EXT} following from Eq 6 is also constant and $\sigma_{EXT} = E_1(e_{EXT} - Ke_{EXT}^2)$.

Both cases *a* and *b* can be represented in Fig. 11 by a general $\sigma(e)$ curve given by Eq 6. In case *a*, the residual stress σ_R and the corresponding deformation e_R are represented by one point P on this curve for compressive residual stresses (or by P' for tensile residual stresses). In case *b*, the $\sigma_{EXT}(e_{EXT})$ dependence (without residual stresses) is, of course, identical with the $\sigma(e)$ curve with respect to the zero point $\sigma = 0$ and $e = 0$.

- However, if the external deformation e_{EXT} is exerted on the coating with a given initial deformation ε_R, the origin of the $\sigma_{EXT}(e_{EXT})$ curve will be displaced with respect to the origin of the $\sigma(e)$ curve to the point P (or P') corresponding to ε_R and σ_R , as shown in Fig. 11. New coordinates for the $\sigma_{EXT}(e_{EXT})$ dependence are plotted in Fig. 11 by dashed lines.

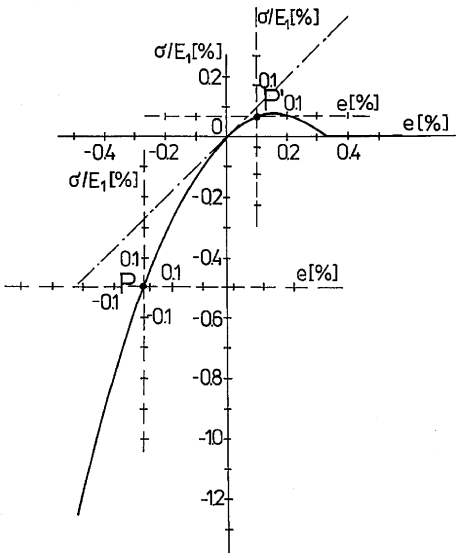

Fig. 11 Combination of residual and external stresses in a thin coating on a thick substrate

The function $\sigma_{EXT}(e_{EXT})$, using the new coordinates, will be different from the plot $\sigma(e)$ in the original coordinates. The given deformations $e_R = -\varepsilon_R$ and e_{EXT} (exerted by the linear substrate deformation) sum up to the resulting deformation $e_R + e_{EXT}$ so that the constant total stress $\sigma_T = E_1[(e_R + e_{EXT}) - K(e_R + e_{EXT})^2]$. The total stress can be divided into two parts, $\sigma_T = \sigma_R + \sigma_{EXT}$, where σ_R is the original constant residual stress and σ_{EXT} is the stress measured during external loading, growing from zero. Therefore, the external stress can be written as:

$$\sigma_{EXT} = E_1[(e_R + e_{EXT}) - K(e_R + e_{EXT})^2] - \sigma_R$$
$$= E_1[e_{EXT} - K(e_{EXT}^2 + 2\,e_R\,e_{EXT})] \quad \text{(Eq 16)}$$

and depends on the initial deformation $\varepsilon_R = -e_R$.

Tangent and secant moduli under external stress in specimens with initial deformations follow as:

$$E^{TAN} = d\sigma_{EXT}/de_{EXT} = E_1[1 - 2K(e_{EXT} + e_R)]$$
$$E^{SEC} = \sigma_{EXT}/e_{EXT} = E_1[1 - K(e_{EXT} + 2e_R)] \quad \text{(Eq 17)}$$

and are also functions of initial deformation $\varepsilon_R = -e_R$.

6. Comments on Fracture under Tensile Stresses

With increasing tensile stresses σ, a mesoscopic crack crossing the whole splat and approximately perpendicular to the direction of σ may develop inside a splat from the microcrack network. Under even higher tensile stresses σ, the extension of the mesoscopic crack from one splat into the neighboring splats will take place and the nucleus of a macroscopic vertical crack will be formed. The formation of the vertical cracks is, from a microscopic point of view, a process of coalescence of intrasplat microcracks. The crack nucleus usually takes the form of an elongated surface crack of small depth d (Fig. 12). Macrocracks perpendicular to the interface develop in coatings under higher tensile stresses, during tensile deformation or bending of the substrate with a coating on the tension face (Fig. 12d-f). New macrocracks are formed with increasing substrate deformation and the coating separates into blocks (Ref 33).

Crack propagation under bending was studied in zirconia thermal barrier coatings (Ref 34) and nonlinear tensile stress–strain curve was measured from small stresses to fracture.

The final stage of a macroscopic crack penetrating the whole thickness of a zirconia coating and even of the metal bond coat (Ref 33) is shown in Fig. 13. The surprizing penetration of the crack into the metal NiCr bond coat may be due to the fact that in this case the bond coat was prepared by air plasma spraying so that the splats were covered by oxides leading to a very brittle bond coat. On the other hand, the crack does not penetrate into the steel substrate and deviates along the bond coat–substrate interface.

While the behavior of coatings and freestanding parts under compressive stresses is similar, the process of fracture under higher tensile stresses is very different. In freestanding parts under stress-driven loading, a critical crack is formed after a small, approximately elastic deformation of the order 0.02–0.04% and brittle fracture follows (Ref 35,36). On the other hand, sprayed ceramic coatings on substrates are deformed under strain-driven loading (controlled by the substrate deformation) and retain their integrity by constraint to the substrate up to larger deformations, of about 0.5% (as proposed in Fig. 4), when already macroscopic cracks are formed; however, the coating still adheres to the substrate. Nevertheless, the average stress σ in the coating approaches zero (Fig. 4).

The extension of a coating crack in the direction to the interface with a substrate having different elastic constants has been studied as a plane strain problem using the fracture mechanics by different authors, quoted e.g., in the review article (Ref 37). As soon as the crack reaches the interface, it can stop there, propagate along the interface or penetrate into the substrate.

The stress intensity factor K_I for a crack of length a in the coating of thickness h is calculated numerically for chosen combinations of elastic constants as a function of dimensionless crack length a/h in Ref 38. Only the case

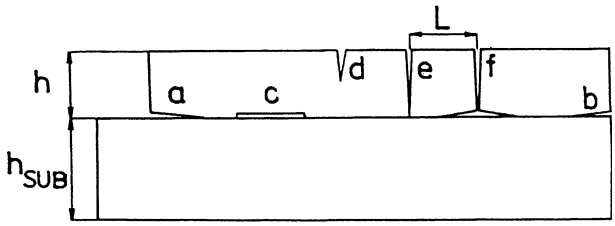

Fig. 12 Fracture (d, e, f) and delamination (a, b, c) of a coating

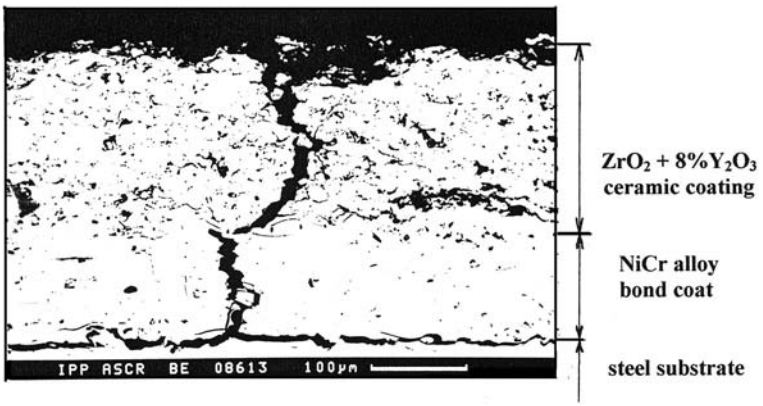

Fig. 13 Macroscopic crack in $ZrO_2 + 8$ wt.% Y_2O_3 coating, penetrating into the NiCr bond coat and deviating along the steel substrate interface. The crack is open due to plastic bending of the steel substrate; the plastic elongation at the substrate interface is 0.8% (Ref 33)

where the crack is repelled by the interface is treated ($E_1 << E_S$). The method of finite elements is used, which is also applied for computation of the stresses induced in front of the crack.

When the crack tip approaches the interface, high tensile stresses σ_{zz} and smaller shear stresses σ_{xz} are induced by the crack in the interface. Decohesion in the interface is formed by these stresses in front of the crack tip and the crack in the ceramic coating reaches the interface, in a similar fashion to a crack approaching a free surface. The resulting configuration is a crack deviating along the interface (Fig. 12, 13).

The low bond strength σ_B (or small K_{IC}) of the interface which enables the local decohesion in front of the crack tip (by interconnection of the interface microcracks) and crack deviation into the interface is typical for the air plasma spraying commonly used for ceramics. High tensile stress σ_{zz} in front of the crack tip can also induce short intersplat cracks within the coating by interconnection of the intersplat microcracks. The path of the main vertical crack then shows local horizontal deviations (Fig. 13).

7. Conclusions

It is well-recognized that the mechanical properties of thermally sprayed materials, especially of ceramics, are governed by the presence of two types of mesoscopic defects, thin intersplat voids and intrasplat microcracks. The *main idea of this review* (partly based on the authors results) is the fact that the mechanical properties of sprayed coatings are strongly nonlinear, due to a gradual elastic closing of intrasplat microcracks under compression and to inelastic growth of density of these microcracks under tension.

The theory of *linear elastic properties* at very small stresses, based on small elastic closings or elastic partial openings of microcracks, summarized critically in Chapter 2, explains well the small values of Young's moduli and the elastic anisotropy.

The *nonlinear behavior* under uniaxial compression and uniaxial tension, in directions parallel to the interface, is characterized in Chapter 3 by the formally proposed nonlinear stress–strain relation (6), depicted in Fig. 4. The value of the new dimensionless material constant $K > 0$ characterizes the degree of nonlinearity. The theoretical stress-strain relation describes well the increase of Young's modulus under compression and the decrease of effective modulus under tension. The values of K can be chosen to give a good agreement with experiments.

The theoretical results for *bending* of substrates with nonlinear coatings in Chapter 4 show an important correction of the linear solution, especially for higher stresses, corresponding to higher initial deformations ε and higher external moments M.

The fact that the *combination* of the residual and external stresses is nonlinear is emphasized in Chapter 5. Young's modulus E_1 of the coating, measured from bending of a beam with coating by external moments, may depend on the residual stresses in the coating and this may partly explain different values of E_1 measured by different authors.

The nonlinear behavior of ceramic coatings under tensile stresses, due to inelastic crack growth, transfers at higher stresses into the macroscopic crack formation and *fracture processes*, as mentioned in Chapter 6. In spite of the repulsion of cracks in the ceramic coating by the metal substrate (it is usually $E_1 < E_0$), the concentration of the tensile stresses in front of the crack tip leads to the debonding of the weak ceramic–metal interface (with a lot of microcracks) and the crack deviates along the interface (as shown in Fig. 12 and 13).

There is an important difference between the ceramic coatings and ceramic *free-standing parts* prepared by thermal spraying. The distribution of microcracks and the behavior under compression is similar. However, their behavior under tension is completely different. The coatings are deformed by the strain-driven loading (controlled by the substrate deformation), retain their integrity up to a relatively large strain and the nonlinear behavior and then the special fracture process can

develop. On the other hand, free-standing parts are deformed by the stress-driven loading and, with increasing stress, critical crack will be formed from microcracks at very small deformation (of the order of 0.01%) and brittle fracture will take place, without the preceding nonlinear region.

There is one important difference between the *metal* and ceramic coatings. The relaxation of the quenching stresses in sprayed metals proceeds preferentially by plastic deformation and interface sliding, and intrasplat microcracks are rare. Nevertheless, the Young's moduli E_1 in the direction paralell with the spraying plane are also smaller than Young's moduli of well sintered metals E_0: it is $E_1 \cong (0.4–0.8)\ E_0$ while in ceramics $E_1 \cong (0.1–0.4)\ E_0$. Therefore, the nonlinear behavior of metal coatings should be less pronounced.

The decrease of microcrack density under compression and the increase of microcrack density under tension result in a *remarkable nonlinearity* in the mechanical behavior of plasma-sprayed ceramic coatings. Within a compressive and tensile deformation of a few per mille, the moduli may change by an order of magnitude.

Acknowledgments

The work was supported by the Institutional Research Plan No. AVOZ20430508 and by the Czech Science Foundation Grant No. GACR 106/05/0483.

References

1. L. Pawlowski, The Science and Engineering of Thermal Spray Coatings. J. Wiley, New York, 1995
2. T.W. Clyne and S.C. Gill, Residual Stresses in Thermal Spray Coatings and Their Effect on Interfacial Adhesion: A Review of Recent Work, *J. Therm. Spray Technol.*, 1996, **5**, p 401-418
3. K. Neufuss, P. Chráska, B. Kolman, S. Sampath, and Z. Travníček, Properties of Plasma-Sprayed Freestanding Ceramic Parts, *J. Therm. Spray Technol.*, 1997, **6**, p 434-438
4. F. Kroupa, Effect of Nets of Microcracks on Elastic Properties of Materials (in Czech), *Kovove materialy*, 1995, **33**, p 418-426
5. F. Kroupa, and M. Kachanov, Effect of Microcracks and Pores on the Elastic Properties of Plasma Sprayed Materials, *Proceedings of 19th Internat. Symp. on Materials Science*, V. Carstensen et al., Ed., Roskilde, Riso Nat. Lab., 1998, p 325-330
6. S.H. Leigh and C.C. Berndt, Modelling of Elastic Constants of Plasma Spray Deposits with Ellipsoid-Shaped Voids, *Acta Mater.*, 1999, **47**, p 1575-1586
7. I. Sevostianov and M. Kachanov, Modeling of the Anisotropic Elastic Properties of Plasma-Sprayed Coatings in Relation to Their Microstructure, *Acta Mater.*, 2000, **48**, p 1361-1370
8. R.F.S. Hearmon, An Introduction to Applied Anisotropic Elasticity. Clarendon Press, Oxford, 1961
9. M. Kachanov, Effective Elastic Properties of Cracked Solids: Critical Review of Some Basic Concepts, *Appl. Mech. Rev.*, 1992, **45**, p 304-335
10. M. Kachanov, I. Tsukrov, and B. Shafiro, Effective Moduli of Solids with Cavities of Various Shapes, *Appl. Mech. Rev.*, 1994, **47**, p S151-S174
11. C.-J. Li, A. Ohmori, and R. McPherson, The Relationship between Microstructure and Young's Modulus of Thermally Sprayed Ceramic Coatings, *J. Mater. Sci.*, 1997, **32**, p 997-1004
12. A. Ohmori and C.-J. Li, The Structure of Thermally Sprayed Ceramic Coatings and Its Dominant Effect on the Coating Properties, *Plasma Spraying Theory and Applications*, S. Suryanarayanan, Ed., World Scientific, Singapore, 1993, p 179-200
13. J. Ilavský, A.J. Allen, G.G. Long, S. Krueger, C.C. Berndt, and H. Herman, Influence of Spray Angle on the Pore and Crack Microstructure of Plasma-Sprayed Deposits, *J. Amer. Ceram. Soc.*, 1997, **80**, p 733-742
14. I. Sevostianov, L. Gorbatikh, and M. Kachanov, Recovery of Information of the Microstructure of Porous/Microcracked Materials from the Effective Elastic/Conductive Properties, *Mater. Sci. Eng.*, 2001, **A318**, p 1-14
15. I. Sevostianov, M. Kachanov, J. Ruud, P. Lorraine and M. Dubois, Micromechanical Analysis of Plasma Sprayed TBC: Anisotropic Elastic and Conductive Properties in Terms of Microstructure. Experimental Verification on YSZ Coatings, *Thermal Spray 2003:Advancing the Science and Applying the Technology*, B.R. Marple and C. Moreau, Ed., May 5–8 2003, ASM International, Orlando, Fl, 2003, Vol. 2, p 1557-1563
16. S.A. Ambarcumjan, Bimodular Theory of Elasticity (in Russian). Moskva, Nauka, 1982
17. J.B. Walsh, The Effect of Cracks on the Compressibility of Rocks, *J. Geophys. Res.*, 1965, **70**, p 381-389
18. J.B. Walsh, The Effect of Cracks on the Uniaxial Elastic Compression of Rocks, *J. Geophys. Res.*, 1965, **70**, p 399-411
19. W.F. Brace, Some New Measurements of Linear Compressibility of Rocks, *J. Geophys. Res.*, 1965, **70**, p 391-398
20. Z. Pros, T. Lokajíček, and K. Klíma, Laboratory Approach to the Study of Elastic Anisotropy on Rock Samples, *Pure Appl. Geophys.*, 1998, **151**, p 619-629
21. F. Kroupa and J. Dubsky, Pressure Dependence of Young's Moduli of Thermal Sprayed Materials, *Scripta Mater.*, 1999, **40**, p 1249-1254
22. F. Kroupa and J. Plesek, Nonlinear Elastic Behavior in Compression of Thermally Sprayed Materials, *Mater. Sci. Eng.*, 2002, **A 328**, p 1-7
23. F. Kroupa and J. Plesek, The Effect of Uniaxial Pressure on Elastic Parameters of Plasma-Sprayed Ceramics, *Acta Technica CSAV*, 2002, **47**, p 39-46
24. F. Kroupa, and J. Plesek, Elastic Nonlinearity due to Microcracks in Thermally Sprayed Materials, *Proceedings of Euromech Colloquium 430*, *Formulations and Constitutive Laws for Very Large Strains*, J. Plesek, Ed., 2001, Institute of Thermomechanics, Prague, p 105-115
25. M. Landa, F. Kroupa, K. Neufuss, and P. Urbánek, Effect of Uniaxial Pressure on Ultrasound Velocities and Elastic Moduli in Plasma-Sprayed Ceramics, *J. Therm. Spray Technol.*, 2003, **12**(2), p 226-233
26. V. Harok and K. Neufuss, Elastic and Inelastic Effects in Compression in Plasma-Sprayed Ceramic Coatings, *J. Therm. Spray Technol.*, 2001, **10**(1), p 126-132
27. H. Kauderer, Nichtlineare Mechanik. Springer Verlag, Berlin, 1958
28. J. Nohava and F. Kroupa, Nonlinear Stress-Strain Behavior of Plasma Sprayed Ceramic Coatings, *Acta Technica CSAV*, 2005, **50**, p 251-262
29. T. Wakui, J. Malzbender, and R.W. Steinbrech, Strain Analysis of Plasma Sprayed Thermal Barrier Coatings Under Mechanical Stress, *J. Therm.Spray Technol.*, 2004, **13**(3), p 390-395
30. T. Varis, E. Rajamaki, and K. Korpiola, Mechanical Properties of Thermal Spray Coatings, *Thermal Spray 2001: New Surfaces for a New Millenium*, C.C. Berndt, K.A. Khor and E.F. Lugscheider, Ed., May 28–30, 2001, ASM International, Singapore, 2001, p 993-997
31. A. Materna and F. Kroupa, Bending of Beams with Nonlinear Thermally Sprayed Coatings, *Acta Technica CSAV*, 2003, **48**, p 27-48
32. F. Kroupa and J. Plesek, Bending of Beams with Elastically Non-Linear Coatings, *J. Therm. Spray Technol.*, 2002, **11**(4), p 508-516
33. Z. Převorovský, M. Landa, F. Kroupa, B. Kolman, and V. Kovář, Acoustic Emission of Deformed Plasma-Sprayed Ceramic Coatings (in Czech), *Proceedings of 3rd International Seminar-Application of Acoustic Methods in Evaluation of Properties of*

Materials 96, P. Palček and Z. Trojanová, Ed., Charles University, Prague, 1996, p 49-56
34. A.K. Ray and R.W. Steinbrech, Crack Propagation Studies of Thermal Barrier Coatings under Bending, *J. European Ceram. Soc.*, 1999, **19**, p 2097-2109
35. E.H. Lutz, Plasma Ceramics, *Powder Metallurgy*, 1993, **25**, p 131-137
36. R.J. Damani and E.H. Lutz, Microstructure, Strength and Fracture Characteristics of a Free-Standing Plasma-Sprayed Alumina, *J. European Ceramic Soc.*, 1997, **17**, p 1351-1359
37. J.W. Hutchinson and Z. Suo, Mixed Mode Cracking in Layered Materials, *Adv. Appl. Mechanics*, 1991, **28**, p 63-191
38. F. Kroupa, I. Náhlík, and Z. Knésl, Crack Growth in Thermally Sprayed Ceramic Coatings, *ActaTechnica CSAV*, 2004, **49**, p 149-168